Loughborough University

ARTS ET MÉTIERS ParisTech
Châlons-en-Champagne

LMPF
Laboratoire de Mécanique et Procédés de Fabrication

1. Identification of 3D heterogeneous modulus distribution with the virtual fields method

Dr. Stéphane AVRIL, Prof. Jonathan M. Huntley,
Prof. Fabrice PIERRON and Dr. Derek D. Steele

2. In-vivo measurement of blood viscosity and and wall stiffness in the carotid using PC-MRI

Dr. Stéphane AVRIL, Prof. Jonathan M. Huntley,
and Dr. Rhodri Cusack

Identification of 3D heterogeneous modulus distribution with the virtual fields method

Dr. Stéphane AVRIL, Prof. Jonathan M. Huntley,
Prof. Fabrice PIERRON and Dr. Derek D. Steele

Principle of elastography

$$\mu \nabla^2 u = -\rho \omega^2 u.$$

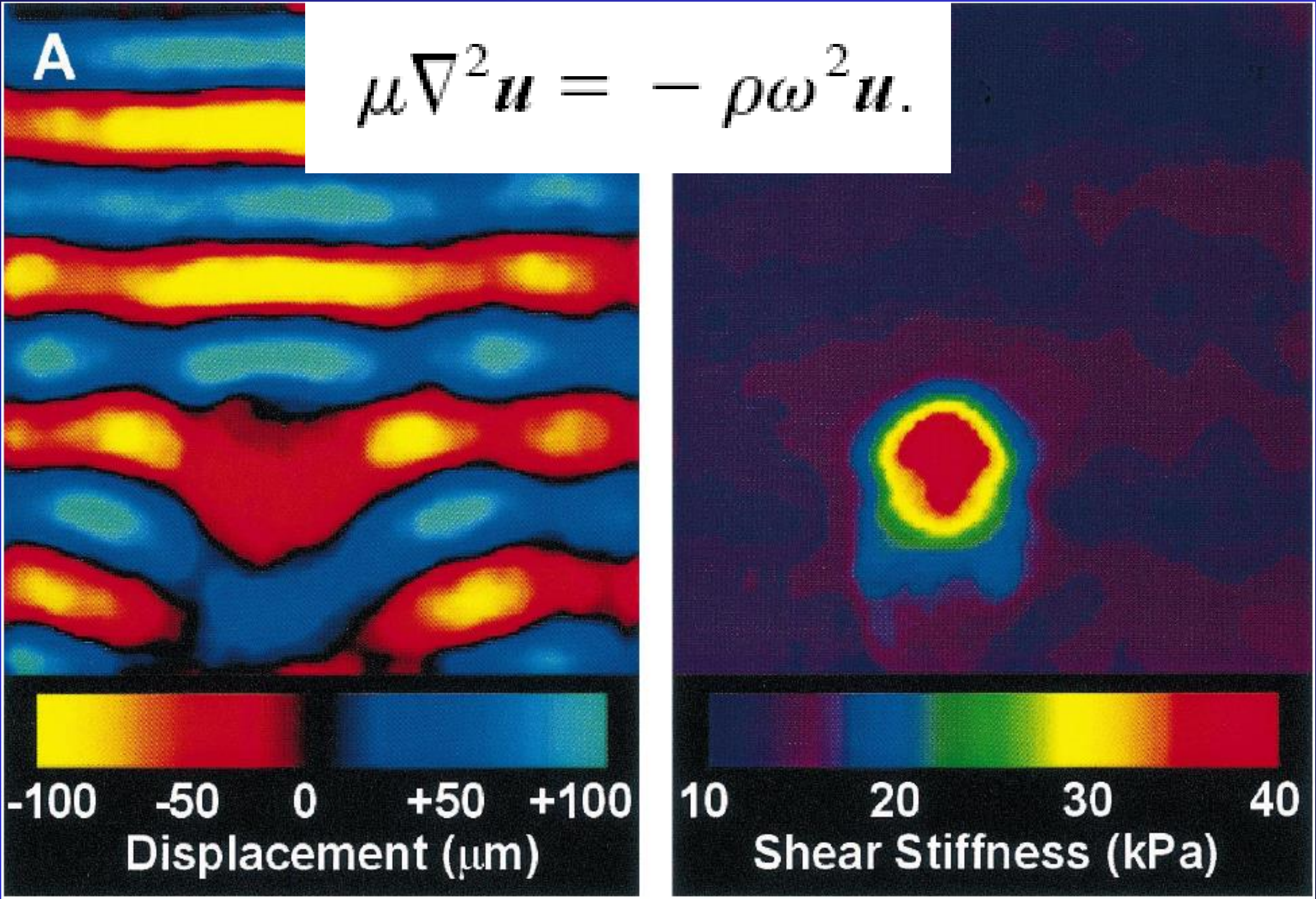

(Manduca et al., 2001)

Issues to solve in static

- Ill posed inverse problems with boundary conditions ;

- $E=\sigma/\varepsilon$ is not correct locally because 3D problem ;

- Large difference between hydrostatic and deviatoric strains because of quasi incompressibility.

- Postprocessing time must be low for real time visualization ;

- Real human tissues have a nonlinear behavior ;

- Measurement issues in medical imaging: noise, synchronisation with loading, magnetic requirements with MRI...

Measurement issues

Breast:

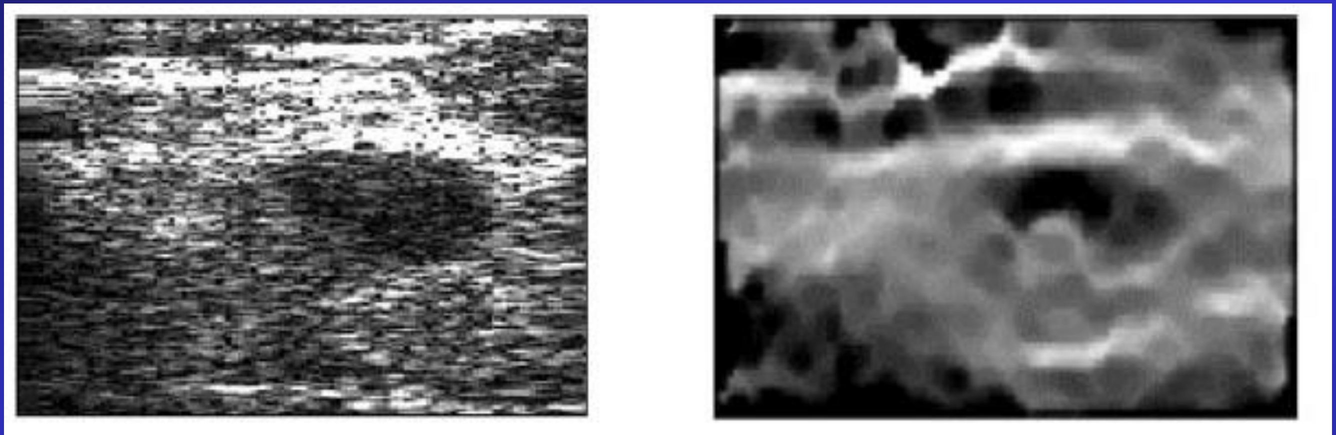

Canine liver:

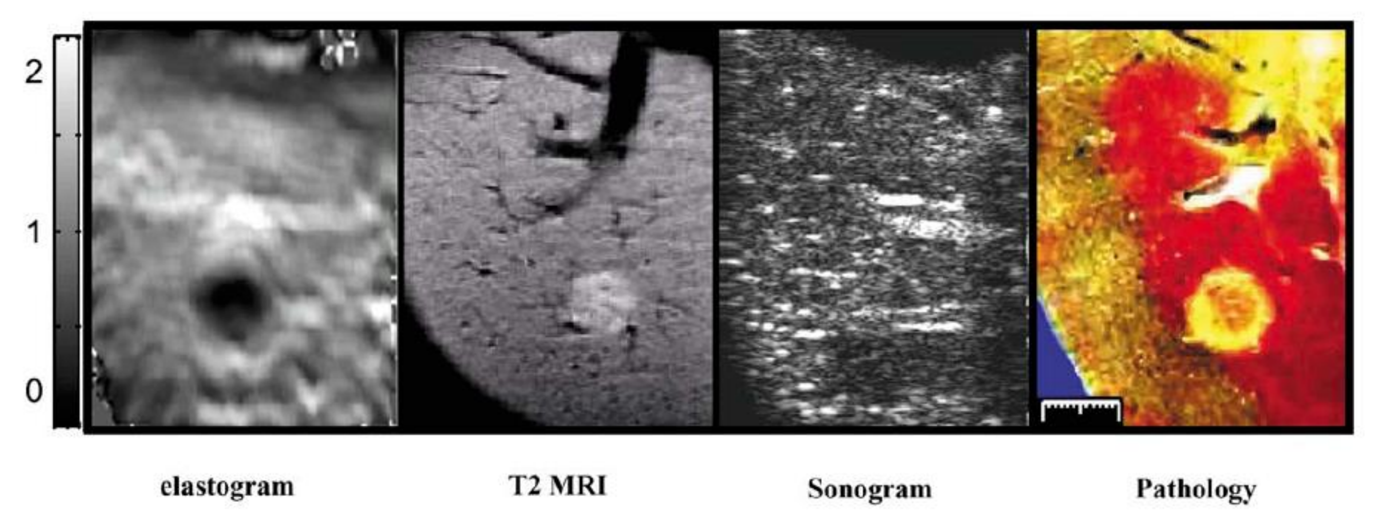

(Ophir et al., 2001)

The virtual fields method: principle

$$-\int_V C_{ijkl}\,\varepsilon_{kl}\,\varepsilon^*_{ij}\,dV + \int_{\partial V} T_i\,u^*_i\,dS = 0$$

measured

chosen

unknown

Discretization of the solid

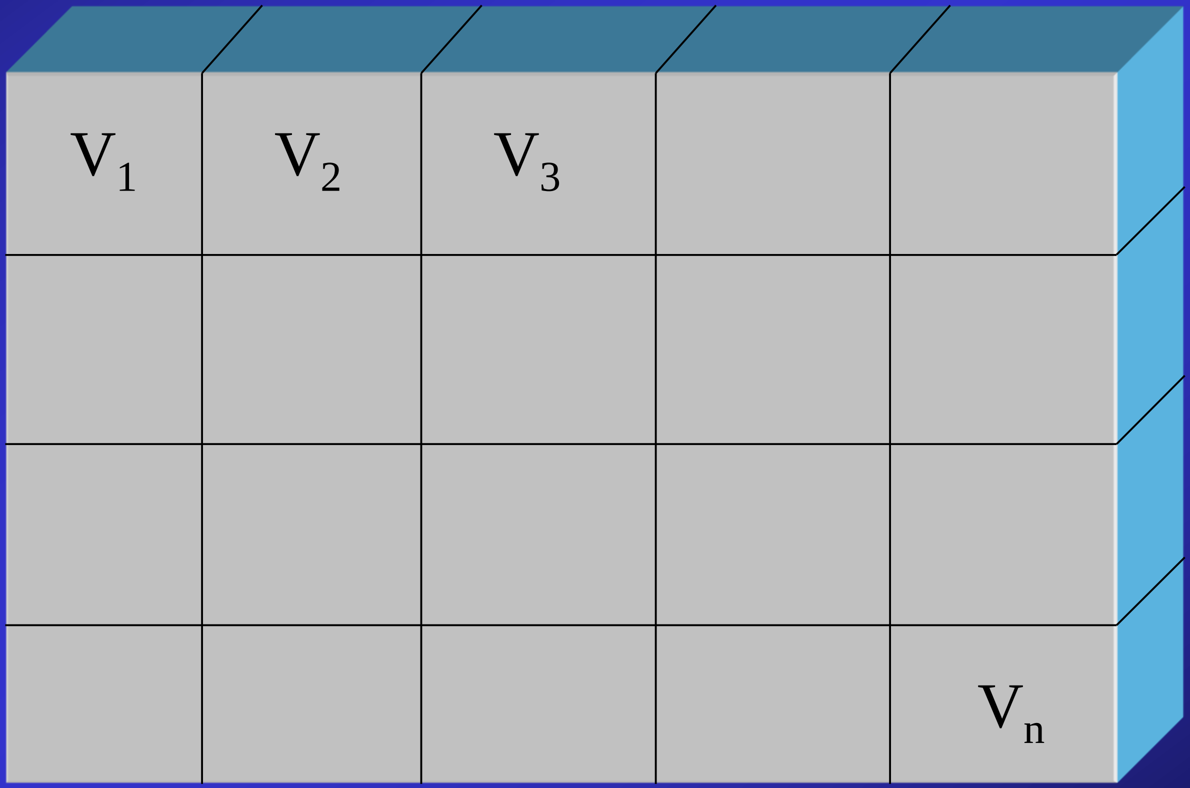

Loughborough University

ARTS ET MÉTIERS ParisTech Châlons-en-Champagne

LMPF Laboratoire de Mécanique et Procédés de Fabrication

Discretization of Hooke's law

$$\begin{Bmatrix} \sigma_{xx} \\ \sigma_{yy} \\ \sigma_{zz} \\ \sigma_{xy} \\ \sigma_{xz} \\ \sigma_{yz} \end{Bmatrix} = \boxed{E}\underbrace{\frac{1-\nu}{(1+\nu)(1-2\nu)} \begin{bmatrix} 1 & \frac{\nu}{1-\nu} & \frac{\nu}{1-\nu} & 0 & 0 & 0 \\ \frac{\nu}{1-\nu} & 1 & \frac{\nu}{1-\nu} & 0 & 0 & 0 \\ \frac{\nu}{1-\nu} & \frac{\nu}{1-\nu} & 1 & 0 & 0 & 0 \\ 0 & 0 & 0 & \frac{1-2\nu}{2(1-\nu)} & 0 & 0 \\ 0 & 0 & 0 & 0 & \frac{1-2\nu}{2(1-\nu)} & 0 \\ 0 & 0 & 0 & 0 & 0 & \frac{1-2\nu}{2(1-\nu)} \end{bmatrix}}_{\text{Constant across the solid}} \begin{Bmatrix} \varepsilon_{xx} \\ \varepsilon_{yy} \\ \varepsilon_{zz} \\ \varepsilon_{xy} \\ \varepsilon_{xz} \\ \varepsilon_{yz} \end{Bmatrix}$$

Piecewise constant

$$\Rightarrow \quad -\sum_{n} E_n \int_{V_n} C^n_{ijkl}\varepsilon_{kl}\varepsilon^*_{ij}\,dV + \int_{\partial V} T_i u^*_i\,dS = 0$$

Choice of virtual fields

Inside nodes, one component is set to 1 and the others to zero alternatively

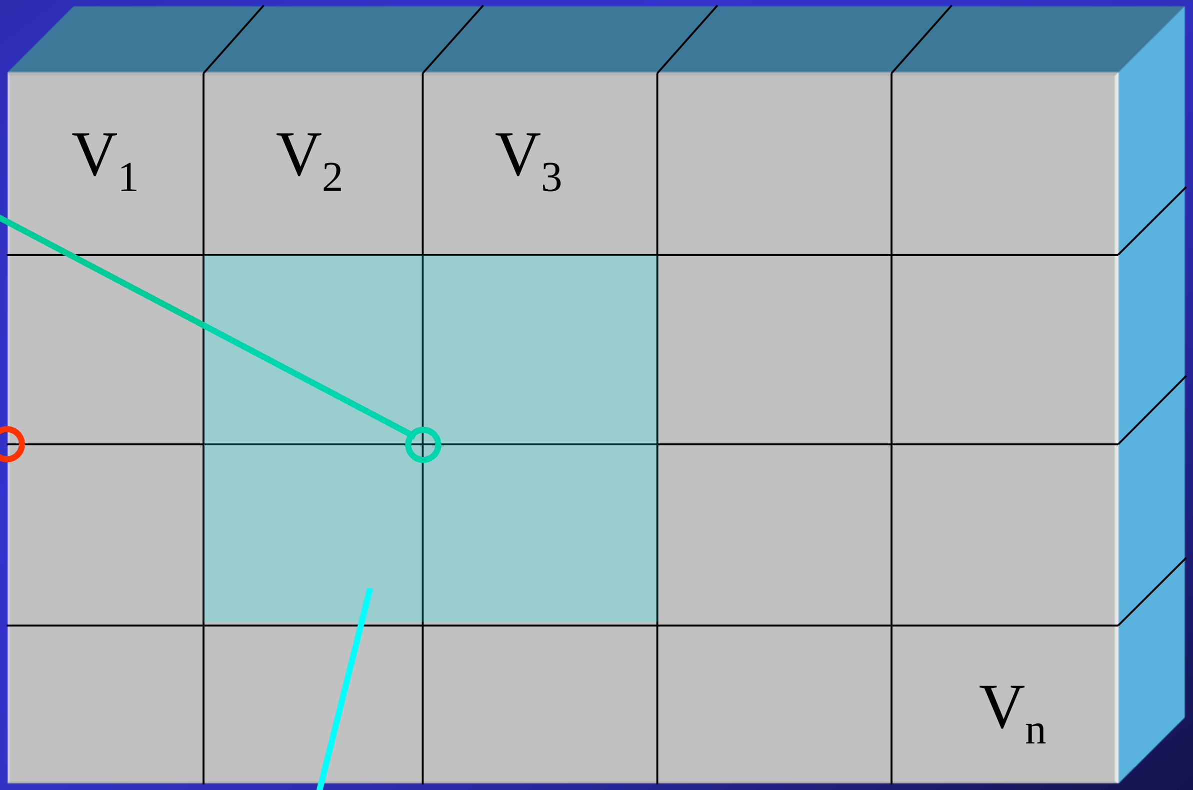

On the boundary, $u_x^*=u_y^*=u_z^*=0$ because unknown reaction forces

Everywhere else using shape functions

Construction of a N x $3N_n$ linear system of equations

$$
\begin{pmatrix}
\int_V \varepsilon_1^* : C^1 : \tilde{\varepsilon} dV & \int_V \varepsilon_1^* : C^2 : \tilde{\varepsilon} dV & \cdots & \int_V \varepsilon_1^* : C^N : \tilde{\varepsilon} dV \\
\int_V \varepsilon_2^* : C^1 : \tilde{\varepsilon} dV & \int_V \varepsilon_2^* : C^2 : \tilde{\varepsilon} dV & \cdots & \int_V \varepsilon_2^* : C^N : \tilde{\varepsilon} dV \\
\vdots & \vdots & \ddots & \vdots \\
\int_V \varepsilon_N^* : C^1 : \tilde{\varepsilon} dV & \int_V \varepsilon_N^* : C^2 : \tilde{\varepsilon} dV & \cdots & \int_V \varepsilon_N^* : C^N : \tilde{\varepsilon} dV
\end{pmatrix}
\begin{pmatrix} E_1 \\ E_2 \\ \vdots \\ E_N \end{pmatrix}
=
\begin{pmatrix} 0 \\ 0 \\ \vdots \\ 0 \end{pmatrix}
$$

Physical interpretation in 1D

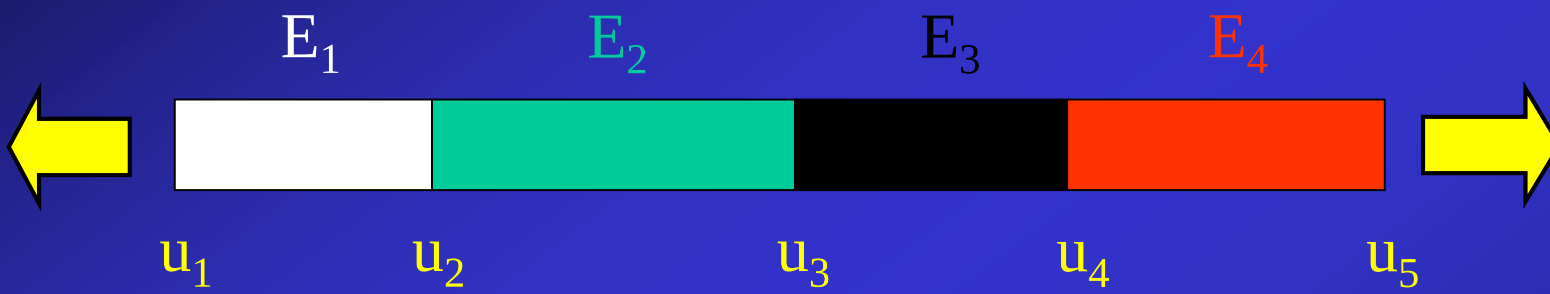

$$\begin{pmatrix} -(u_2-u_1)/L_1 & (u_3-u_2)/L_2 & 0 & 0 \\ 0 & -(u_3-u_2)/L_2 & (u_4-u_3)/L_3 & 0 \\ 0 & 0 & -(u_4-u_3)/L_3 & (u_5-u_4)/L_5 \end{pmatrix} \begin{pmatrix} E_1 \\ E_2 \\ E_3 \\ E_4 \end{pmatrix} = \begin{pmatrix} 0 \\ 0 \\ 0 \\ 0 \end{pmatrix}$$

Numerical resolution

- More equations than unknowns: $3N_n > N$

- Large sparse system: >100000 unknowns

- Resolution in the least square sense

- Iterative resolution using the conjugate gradient method.

- Limited number of iterations of the conjugate gradient method: fast and regularizing.

Experimental arrangements

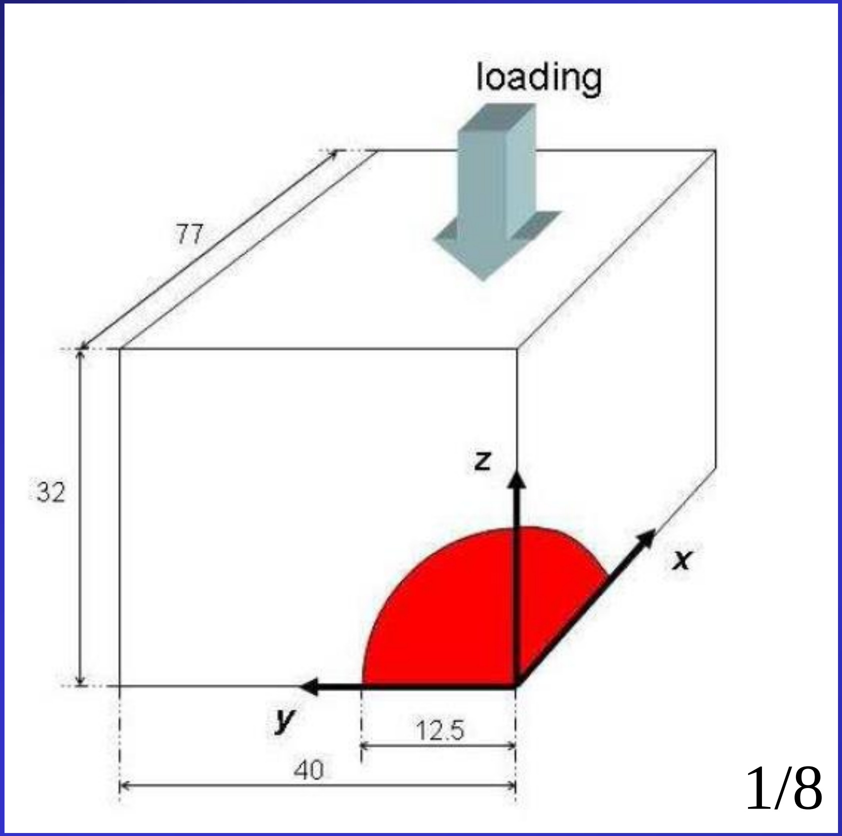

Cube with a stiff inclusion buried in it.

Silicone gel materials mimicking human tissue containing a tumour.

MRI: RF pulse

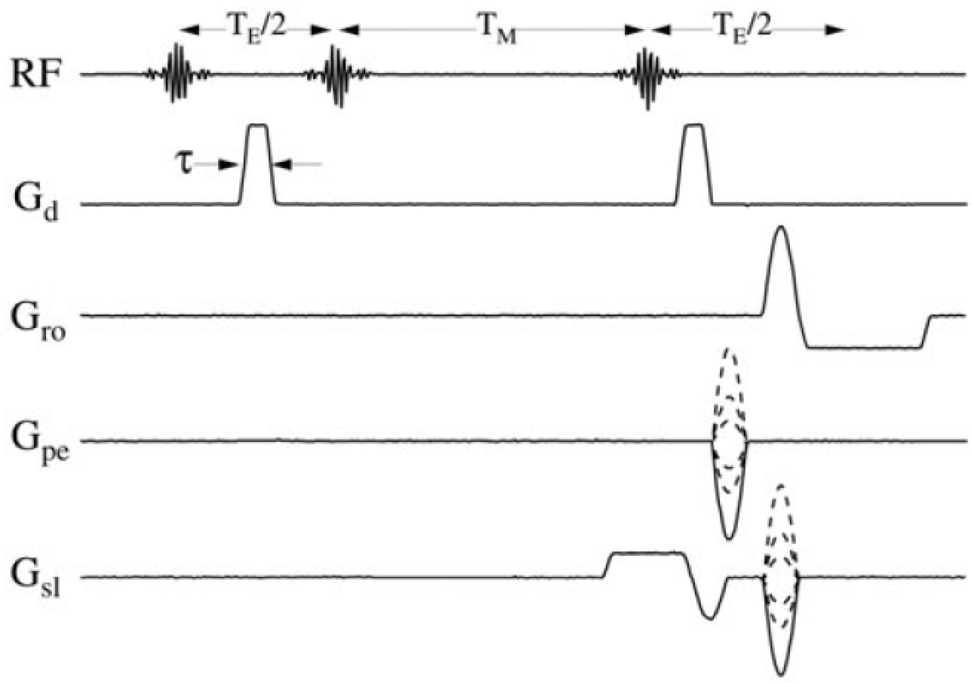

Figure 2. Displacement encoding, stimulated echo pulse sequence waveforms. RF = radio frequency, G_d = displacement encoding gradient, and G_{ro} = read-out (x_1), G_{pe} = phase-encode (x_2) and G_{sl} = slice (x_3) directed gradient waveforms. T_M is the mixing time, T_E is the echo time and τ is the duration of the displacement encoding gradient. Note that the displacement encoding gradient may be applied to any of the directional waveforms.

Displacement fields measured by MRI

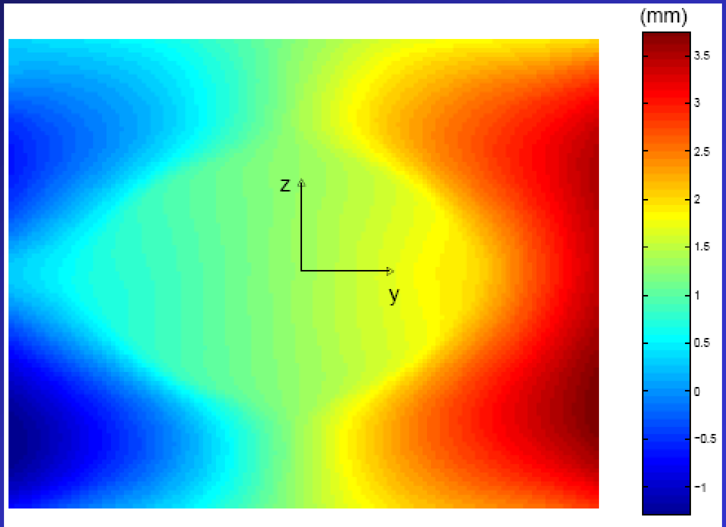

Scanning tomographic method:
→ 3D bulk measurements!!

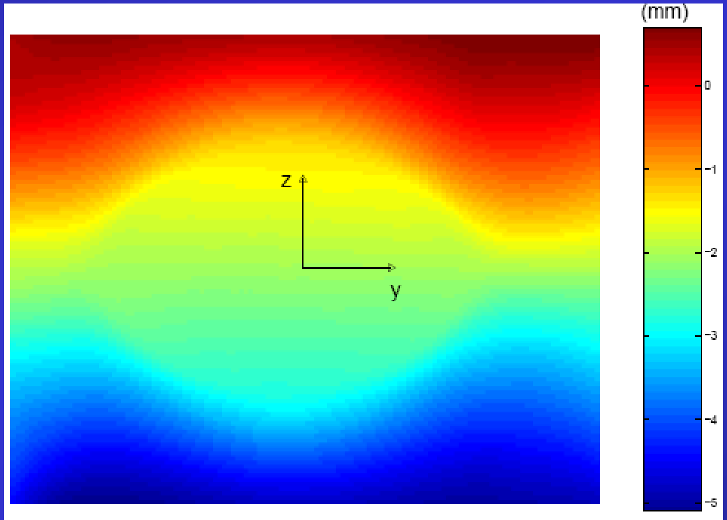

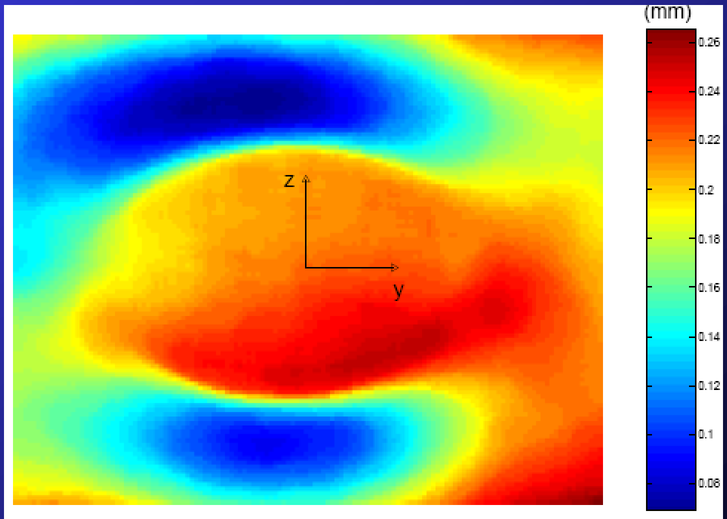

Strain fields

ε_{xx}

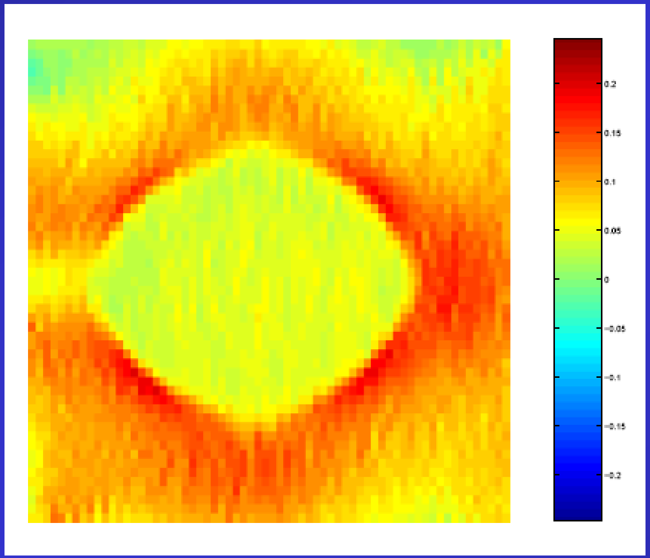

ε_{yy}

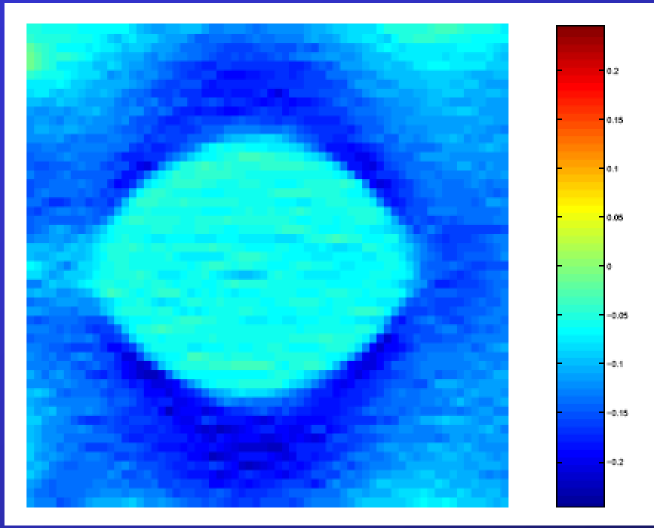

Strain fields

$\varepsilon_{xx} + \varepsilon_{yy} + \varepsilon_{zz}$

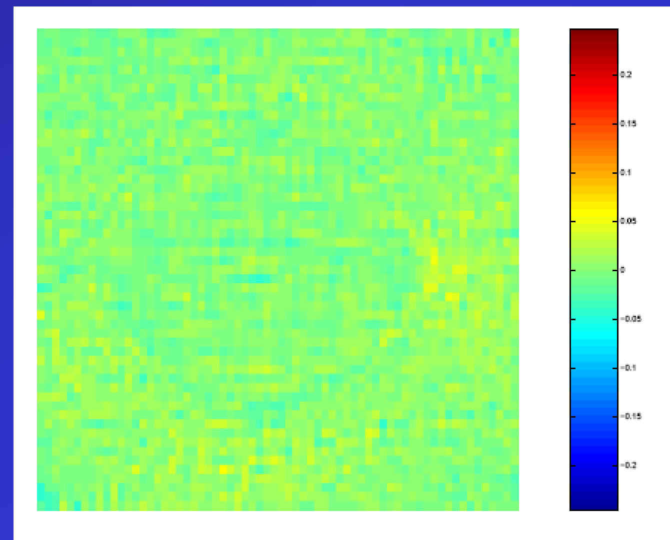

→ incompressibility

→ Hooke's law for incompressible materials

$$\begin{Bmatrix} \sigma_{xx} \\ \sigma_{yy} \\ \sigma_{zz} \\ \sigma_{xy} \\ \sigma_{xz} \\ \sigma_{yz} \end{Bmatrix} = \begin{Bmatrix} p \\ p \\ p \\ 0 \\ 0 \\ 0 \end{Bmatrix} + 2G \begin{bmatrix} 1 & 0 & 0 & 0 & 0 & 0 \\ 0 & 1 & 0 & 0 & 0 & 0 \\ 0 & 0 & 1 & 0 & 0 & 0 \\ 0 & 0 & 0 & 1 & 0 & 0 \\ 0 & 0 & 0 & 0 & 1 & 0 \\ 0 & 0 & 0 & 0 & 0 & 1 \end{bmatrix} \begin{Bmatrix} \varepsilon_{xx} \\ \varepsilon_{yy} \\ \varepsilon_{zz} \\ \varepsilon_{xy} \\ \varepsilon_{xz} \\ \varepsilon_{yz} \end{Bmatrix}$$

3D Results

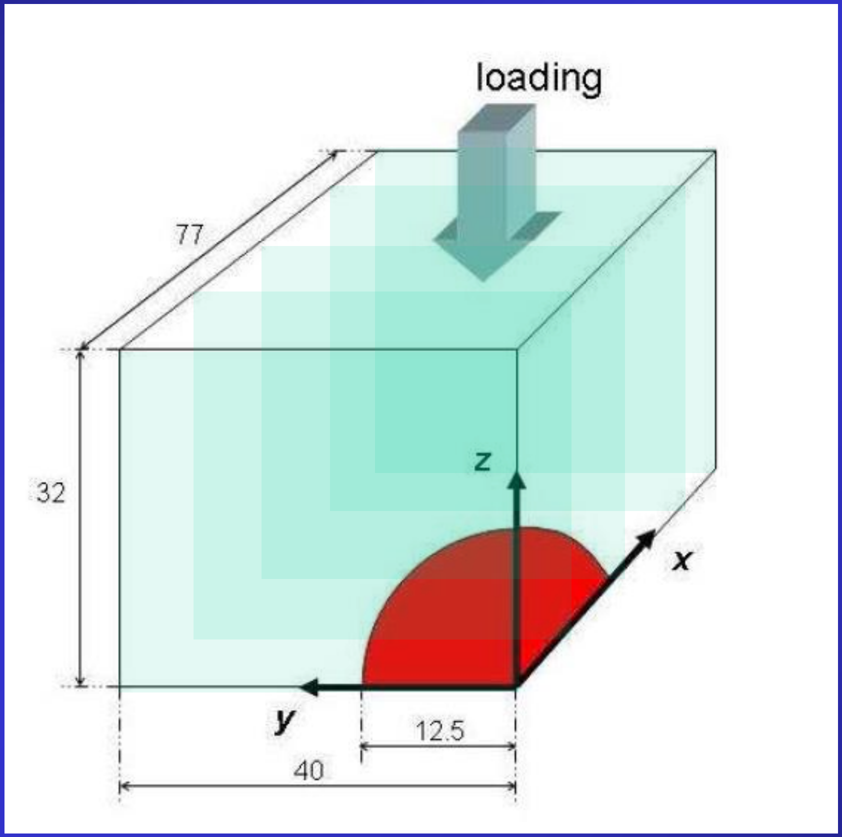

3D Results

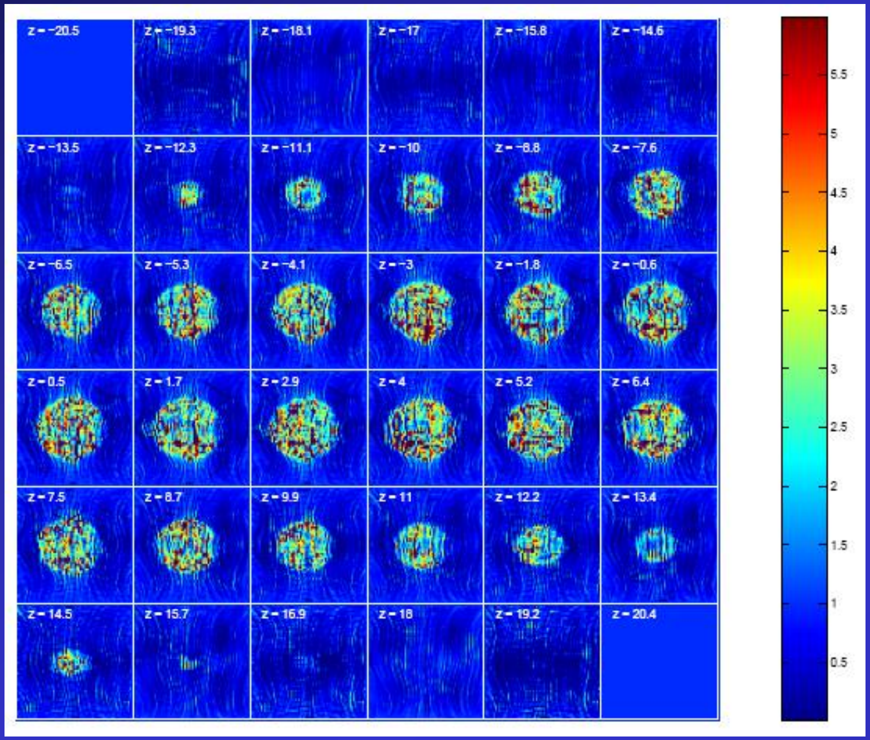

Obtained results after 500 iterations of the CGM = 2 minutes.

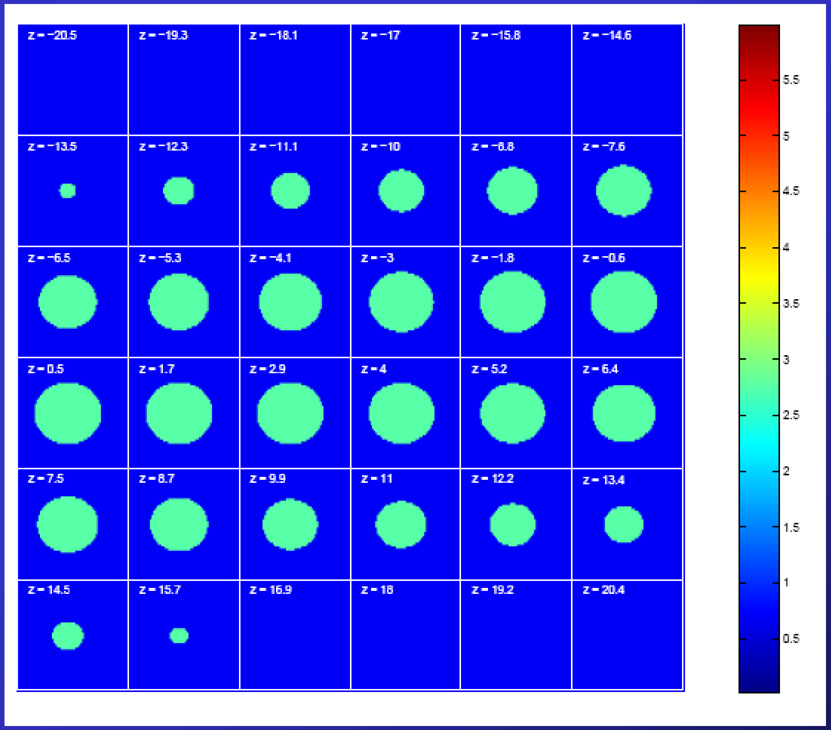

Reference using the actual geometry of the specimen and its properties.

3D Results

Results after median filtering

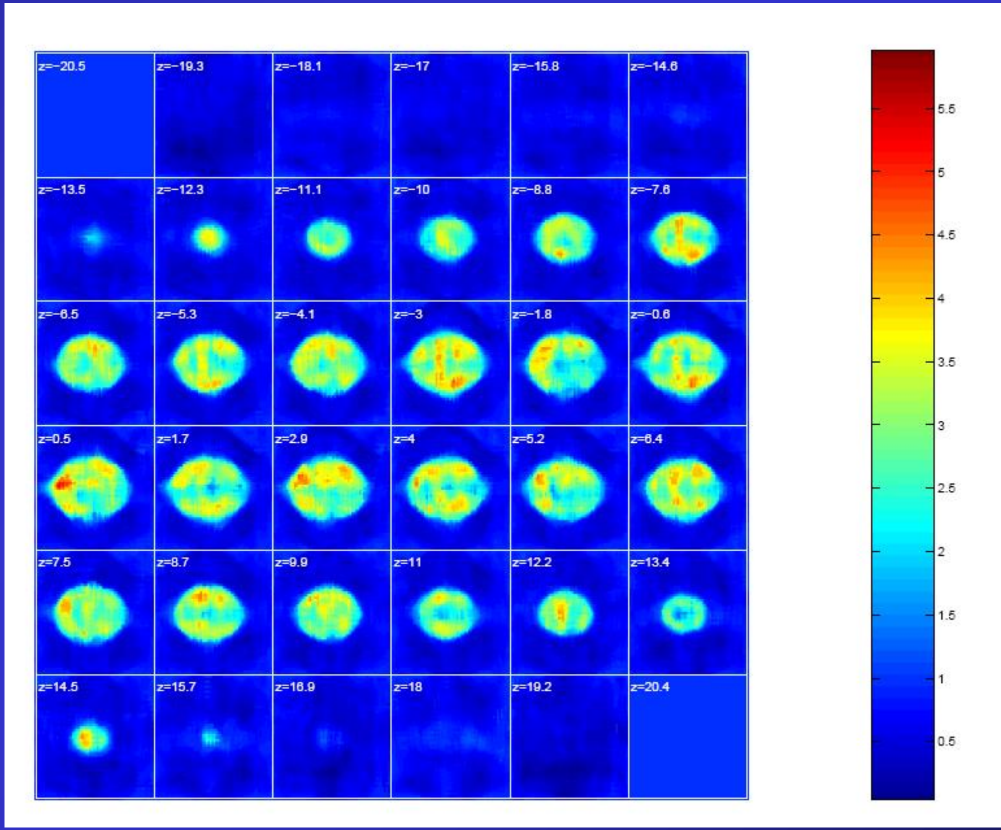

Conclusion and prospects

- Developement of the virtual fields method for reconstruction modulus distribution from ful-field data

- Application to post-processing of medical images.

- Implementation of regularizing approaches in progress.

In-vivo measurement of blood viscosity and and wall stiffness in the carotid using PC-MRI

Dr. Stéphane AVRIL, Prof. Jonathan M. Huntley,
and Dr. Rhodri Cusack

MRI applied to a cross section of the neck

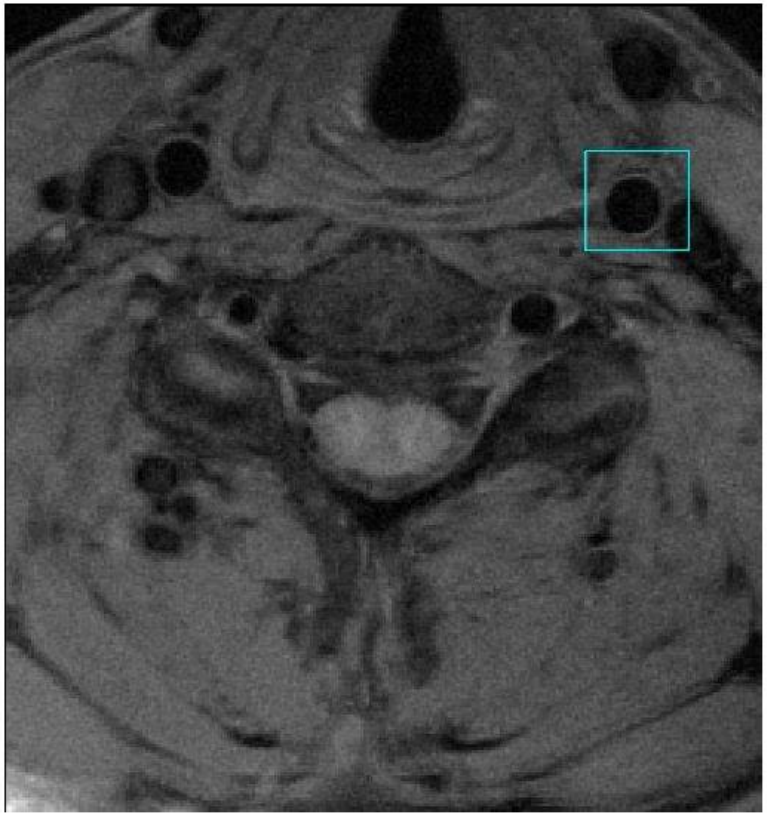

(a) Whole neck cross-section (black-blood sequence)

Principle of time resolved PC-MRI

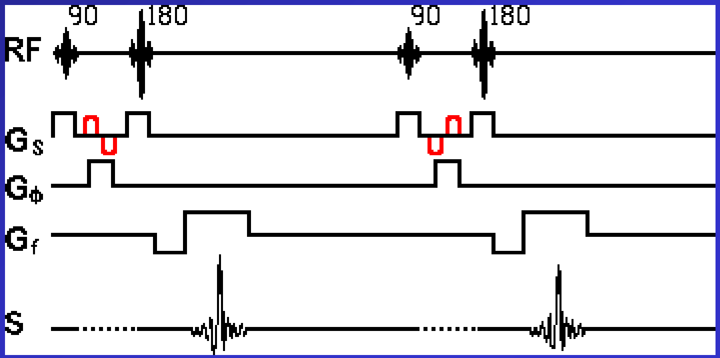

RF pulse sequence

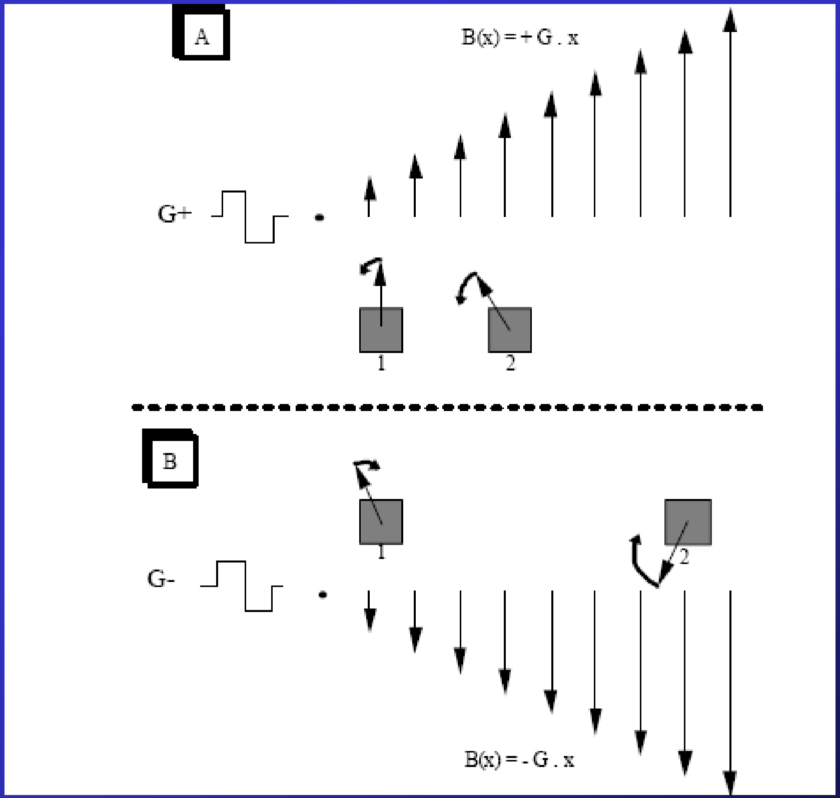

Principel of velocity encoding

Time resolved PC-MRI applied to a patient's neck: signal magnitude

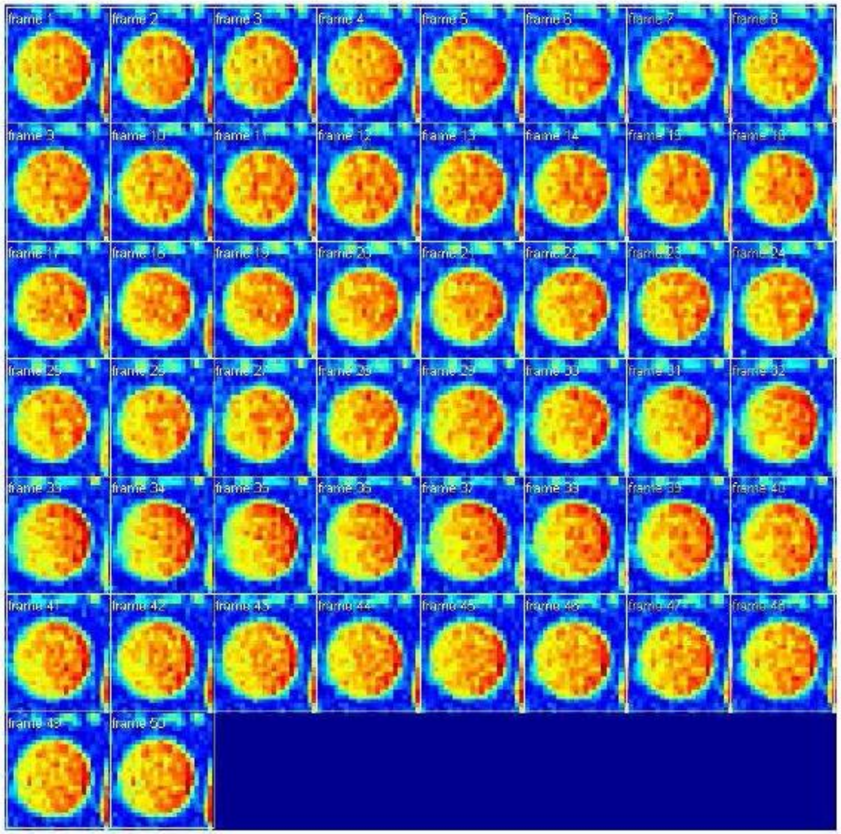

(b) Frames of signal magnitude

Time resolved PC-MRI applied to a patient's neck: velocity maps

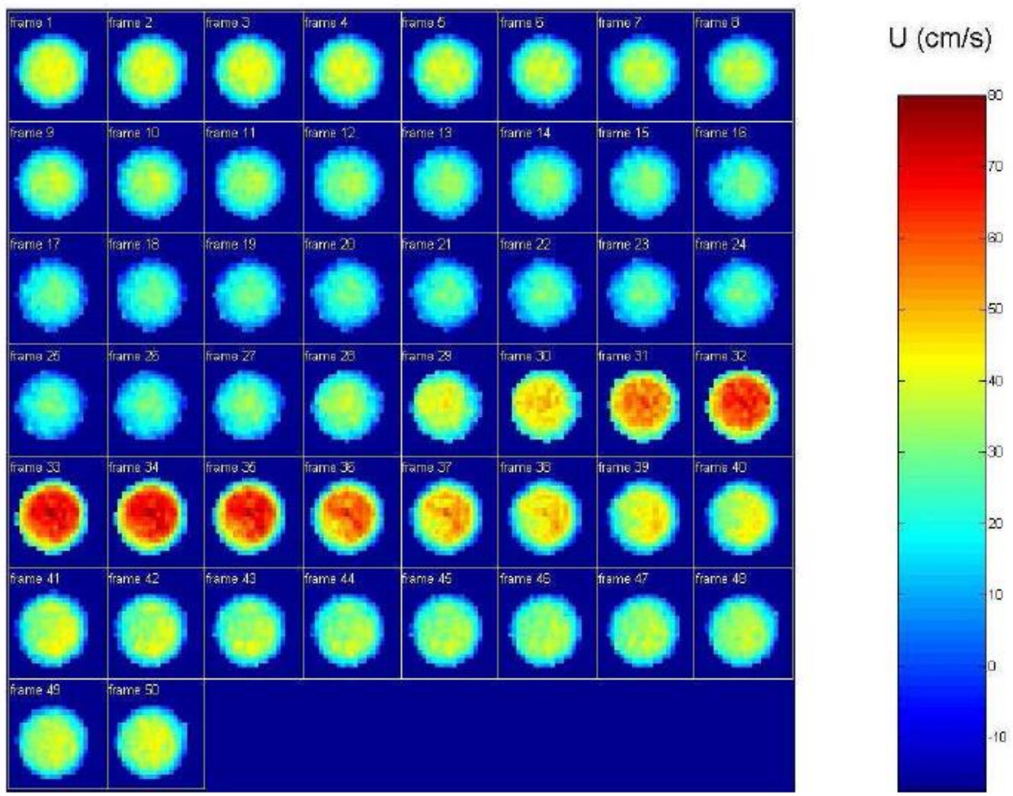

(a) 50 velocity frames in the carotid

Model calibration for deducing the blood viscosity

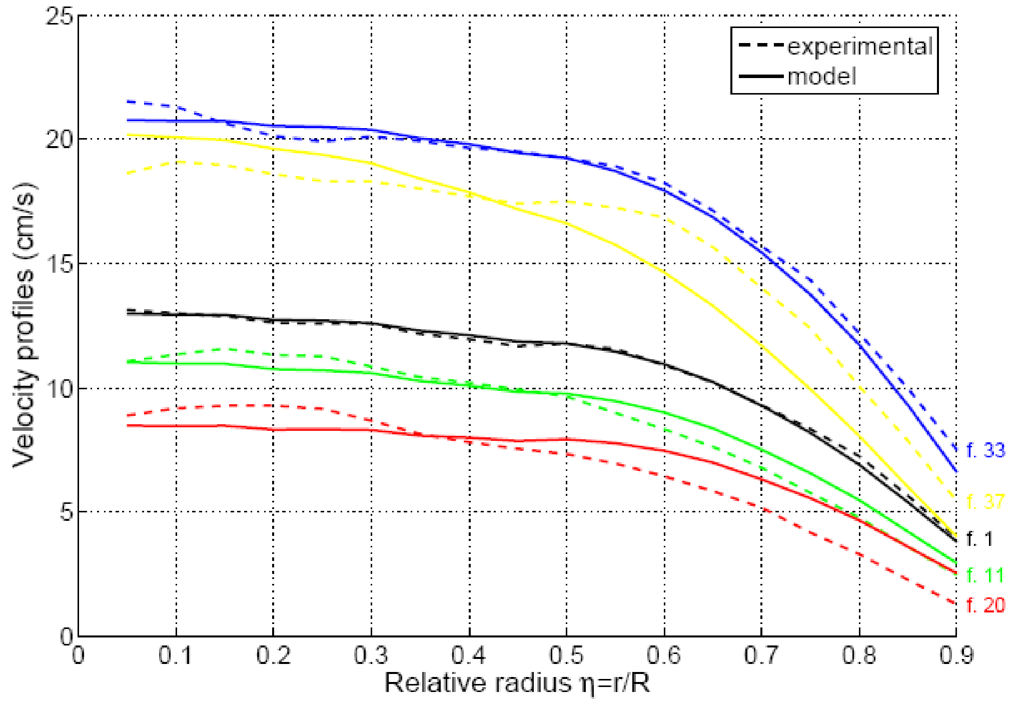

(b) Profiles of the velocity for a few frames.

$\mu = 0.0073$ Pa.s

Model calibration for deducing the pulse wave velocity

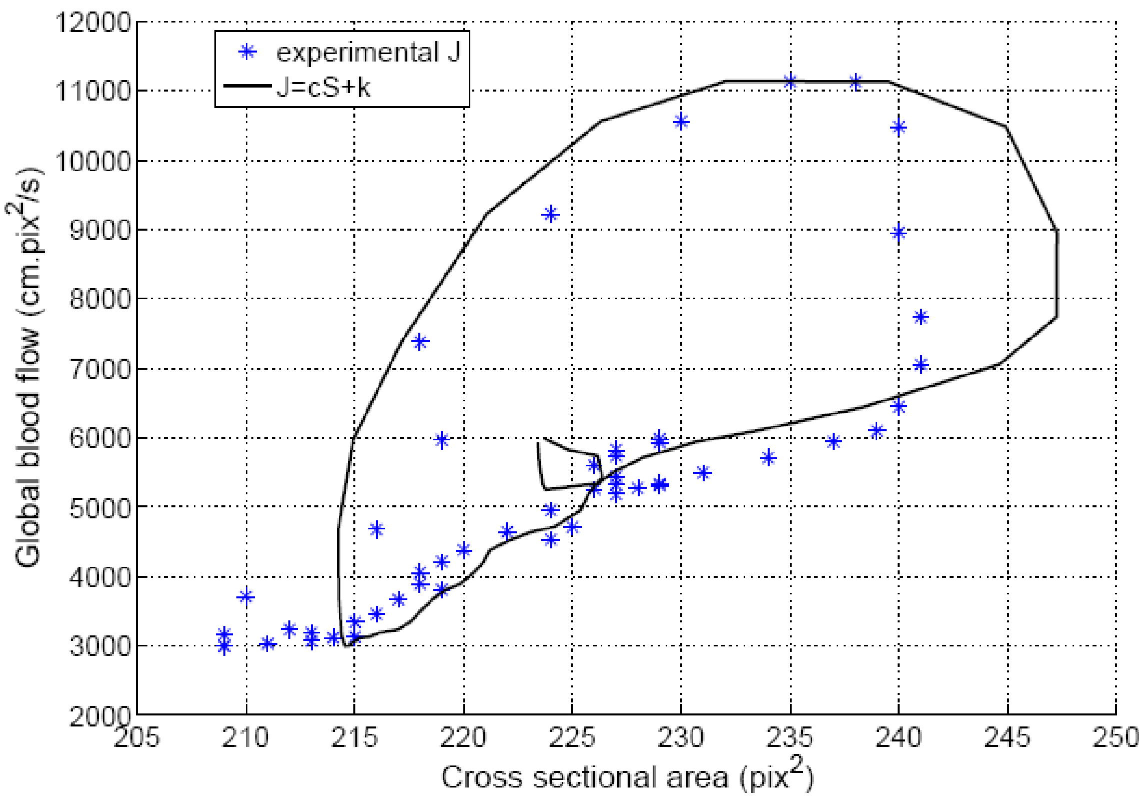

(a) J versus S

Model calibration for deducing the pulse wave velocity

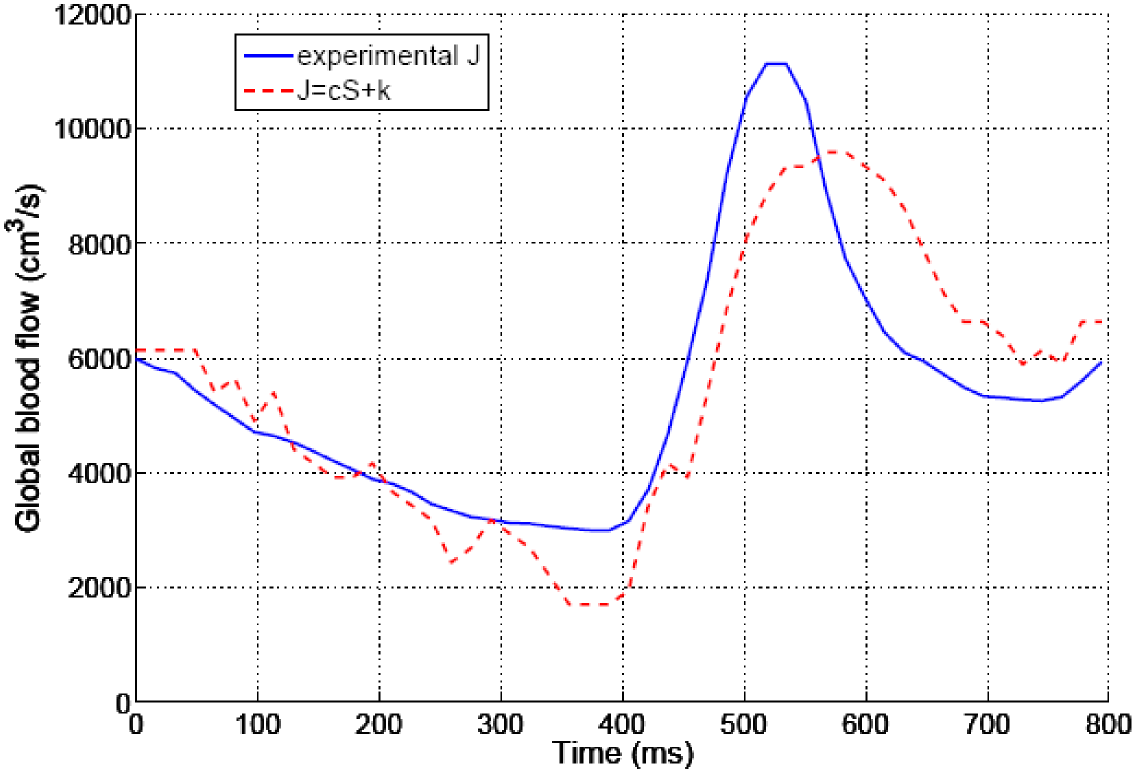

(b) J versus t

c = 2.7 m/s (right)

c = 4.1 m/s (left)

Identification of the wall stiffness using the Moens-Korteweg equation

$$E = \frac{2\rho c^2 R_0}{h}$$

E = 99 kPa (right)
E = 150 kPa (left)

Prospects: extension to plaques
=
heterogeneous mechanical properties